

# A step towards testing general relativity using weak gravitational lensing and redshift surveys

Yong-Seon Song<sup>1</sup> and Olivier Doré<sup>2\*</sup>

<sup>1</sup>*Institute of Cosmological & Gravitation, University of Portsmouth, Portsmouth, PO1 3FX, UK and*

<sup>2</sup>*Canadian Institute for Theoretical Astrophysics, 60 St. George St,*

*University of Toronto, Toronto, ON, Canada M5S3H8*

(Dated: May 20, 2021)

Using the linear theory of perturbations in General Relativity, we express a set of consistency relations that can be observationally tested with current and future large scale structure surveys. We then outline a stringent model-independent program to test gravity on cosmological scales. We illustrate the feasibility of such a program by jointly using several observables like peculiar velocities, galaxy clustering and weak gravitational lensing. After addressing possible observational or astrophysical caveats like galaxy bias and redshift uncertainties, we forecast in particular how well one can predict the lensing signal from a cosmic shear survey using an over-lapping galaxy survey. We finally discuss the specific physics probed this way and illustrate how  $f(R)$  gravity models would fail such a test.

PACS numbers:

## I. INTRODUCTION

To understand the origin of the accelerating expansion of the universe is one of the salient question in contemporary cosmology [1, 2, 3, 4, 5, 6, 7]. It is commonly attributed to the existence of some extra unknown physics loosely labelled Dark Energy (DE) [8]. Alternatively, it might cast some doubts on the theoretical foundation of current cosmology, that is the theory of General Relativity (GR). From a theorist point of view, as most efforts to construct self-consistent DE models within GR seem unsuccessful, there is no a priori reason to rule out a modification to gravity on cosmological scales as an explanation [9]. From an observer point of view, whereas GR passes direct tests probing the Solar System scales ( $10^{11}$ m) down to the laboratory scales ( $10^{-3}$ m) [10], testing gravity on cosmological scales is challenging and overly model dependant so far. In this work, we propose to remedy these issues by defining a set of simple model independent tests of GR on cosmological scales, although more complicated models of GR (clumping dark energy or interacting dark energy models) are not considered in this paper (the complete set of test including both exotic dark energy models is being prepared as the second step of testing gravity). The tests we devise rely on simple and testable consistency relations based on linear GR and make use of the appropriate combinations of various observables of large scale structures. Were any of these relations proved to be violated, it would be a clear sign of a break-down of GR and it would highly motivate theoretical work on alternatives to GR. Reversely, before any such conclusion can be reached, it requires an absolute demonstration that observational systematic effects are well under controlled.

A firm believer in GR might look at these states as simple test of systematic effects. Note that throughout this work, we will assume the validity of standard cosmology, that is to say the validity of the Copernican principle [11]. If this was not the case, then the DE problem could be solve without new physics and more specific tests would have to be designed [12, 13, 14].

Several alternative approaches to test GR have been proposed so far, some parametric, some non-parametric. The parametric approaches can be classified into several categories according to their goal: i) to separate the geometrical and growth signatures in the  $w$  &  $w_a$  plane [15, 16, 17], ii) to define the probed  $w(z)$  range in a model independant manner [18, 19, 20], iii) to look for an anomalous linear growth rate using the  $\gamma$  parameter [19, 21, 22, 23, 24, 25, 26, 27], iv) to parametrize the metric perturbations [28, 29, 30, 31, 32, 33, 34, 35, 36, 37, 38, 39, 40]. Alternatively, non-parametric approaches were developed by [41, 42, 43, 44].

In this paper, we advocate the use of a non-parametric approach – based on a set of GR based consistency relations – to test gravity on cosmological scales. We will use explicit alternative to GR for illustrative purpose only. To do so, we jointly use various observables, *i.e.* velocities, galaxy clustering and weak-gravitational lensing [41]. More precisely, by using a combination of the two first, we will be able to compare it to the later. In this work, extending the work of [42] we focus closely on potential observational biases. We propose in particular various ways to deal with the galaxy bias, redshift space distortion and spectroscopic and photometric redshifts.

We first begin by introducing in Sec. II a general framework to test GR on cosmological scales. We then detail how to build faithful probes of matter perturbations in Sec. III before detailing one test of GR in Sec.IV. We

---

\*Electronic address: Yong-seon.song@port.ac.uk,olivier@cita.utoronto.ca conclude and discuss our findings in Sec. V.

## II. GRAVITATIONAL CONSISTENCY TESTS ON COSMOLOGICAL SCALES

In a metric theory of gravity, large scale structures correspond to metric and matter-energy momentum perturbations. In the Newtonian gauge, metric perturbations are described by

$$ds^2 = -(1 + 2\Psi)dt^2 + (1 + 2\Phi)a^2\delta_{ij}dx^i dx^j, \quad (1)$$

where  $\Phi$  and  $\Psi$  denote curvature perturbations and the Newtonian force respectively. In this work (except in section Sec. IV B) we will aim at constructing GR consistency relations and thus we will work within GR. We will restrict ourselves to a linear theory of perturbations on sub-horizon scales to get simpler and easier to test relations. We will also consider matter density fluctuations to be dominating the growth of perturbations and thus neglect DE clustering.

The first simple relation that can be tested within GR is based on the continuity equation:

$$\frac{d\delta_m}{dt} = -\frac{\theta_m}{a} \quad (2)$$

where  $\theta_m$  is given by  $\theta_m = \vec{\nabla} \cdot \vec{v}_m$ . Both sides of this equation can be probed observationally independently and we shall call the observational test of this relation the *energy-momentum consistency test*. As will be seen below, whereas peculiar velocities can be traced directly, probing matter density fluctuations requires to deal with several observational artifacts. In this paper, we will assume this relation to be satisfied and we will use it for our observational determination of the galaxy bias. Note however that it could be violated due to dark sector interactions.

The second consistency relation stems from the lack of anisotropic stress and relates metric perturbations. Since in this paper, we neglect DE clustering, only the matter component clusters and the no anisotropic stress approximation is valid,

$$\Phi + \Psi = 0, \quad (3)$$

which reduces the degrees of freedom of metric perturbations. While the Newtonian force  $\Psi$  can be reconstructed from the evolution of peculiar velocities, the curvature perturbation  $\Phi$  is given by matter fluctuations. Thus both observables could be compared to determine the presence of non-trivial anisotropic stress which is predicted in most modified gravity models and dark energy clumping model. We call this test the *metric consistency test*.

The other tests relate metric perturbations to matter-energy fluctuations, dynamically or non-dynamically. Newtonian force sources the dynamics of matter fluctuations. If the time evolution of peculiar velocity can be reconstructed, then so can  $\Psi$  through the Euler equation,

$$\frac{d\theta_m}{dt} = -H\theta_m + \frac{k^2\Psi}{a}, \quad (4)$$

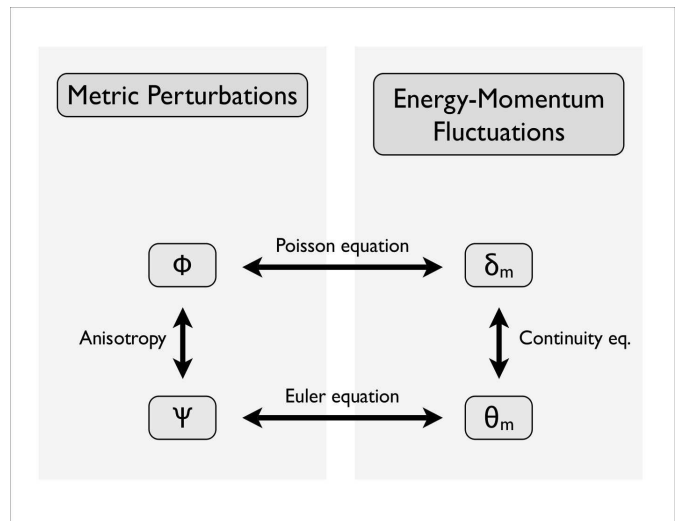


FIG. 1: Web of cosmological tests of GR (see an analogous plot in Fig. 1 of [33]).

which we label as the *dynamical constraint test*. Because the degrees of freedom available in metric perturbations are reduced by the no-anisotropy condition in GR, we shall not use this constraint in this paper.

Finally, the relation between curvature perturbations and matter fluctuations yield the *non-dynamical constraint test*, also known as the Poisson equation. It is a key relation which we will use and test in this work. It writes as,

$$k^2\Phi = 4\pi G a^2 \rho_m \delta_m. \quad (5)$$

Using previously defined relations, in principle both sides of Eq. 5 are calibrated and can be readily used to test it.

This set of relation constitute a web of possible cosmological as illustrated in Fig. 1.

As we hinted at before, to test any of this relations, we need various observables. To trace matter perturbations,  $\delta_m$ , we will use biased tracers like galaxies or clusters, whose relevant observational caveats will be addressed below. Velocity surveys, direct (kinetic Sunyaev-Zel'dovich or peculiar velocities measurements) or indirect (galaxy redshift survey) allow us in principle to probe  $\theta_m$ . Finally, metric perturbations are directly probed by weak gravitational lensing which distorts the shape of source galaxies along the line of sight. Since the geodesics are determined by the gradient of combination of both  $\Phi$  and  $\Psi$ , as  $\nabla(\Phi - \Psi)$ , weak lensing will probe the integrated effect of metric combination which is  $2\nabla\Phi$ . We will introduce our notations for those observables below before discussing in more details the specifics of the test we are interested in.

### III. TRACING MATTER PERTURBATIONS WITH GALAXIES

Whereas there is no direct probe of matter density fluctuations (even though peculiar velocity measurements are usually considered to be a direct tracer of density fluctuations, this requires the energy momentum conservation law written in Eq. 2 which is not granted in our context), galaxies can still be used for this purpose provided several observational artifacts are properly accounted for.

Since we are working on large linear scales, we will ignore non-linear effects which usually are another limiter. We will nevertheless discuss in the next sections redshift distortions, redshift measurement uncertainties and bias. The information extracted from galaxy density fluctuations will be limited by how well we can handle those effects. Because the tests we are presenting require the use of projected quantities, we will focus in particular on how those artifacts affect the projected galaxy distribution within a redshift bin in its comparison to the projected matter distribution.

In this paper we will restrict ourselves to compare the measured and predicted power spectra, even though a map-based approach would be feasible. As we will work mostly on large scales where the field distribution is Gaussian, considering this approach is lose-less. It is certainly not true on smaller scales.

#### A. Cross-Power spectra conventions

In this work, we are interested in cross-correlating various tracers of the curvature perturbations at various redshifts to test gravity. We will consider three observables based on gravitational lensing, galaxy counts and velocity measurements from redshift-space distortion. In particular, we will sometimes combine some projection of those observables and we will thus define the associated angular power spectra below.

We will consider that the Limber approximation is valid for all those observables in the angular range of interest. The projected angular power spectra  $C_\ell^{XX'}$  of any pair of perturbations  $X$  and  $X'$  is given by

$$C_\ell^{XX'} = \frac{9}{25} \frac{2\pi^2}{(\ell + 1/2)^3} \times \int dD DW^X(D)W^{X'}(D)\Delta_{\zeta\zeta}(a_0, k = \frac{\ell}{D}) \quad (6)$$

where  $\Delta_{\zeta\zeta}(a_0, k)$  is the rms amplitude of curvature fluctuations on comoving hyper-surfaces at the starting epoch  $a_0$  during matter domination and  $D$  is the angular diameter distance. The window function  $W^X(D)$  is determined by the property of the quantity  $X$  as is shown explicitly below.

We consider that galaxies follow a continuous distribu-

tion  $n(z)$ , defined as

$$n_g(z) \propto z^2 e^{-(z/1.5)^2}. \quad (7)$$

where we assume the space-based surveys [45]. We consider that for each observed galaxy, we can measure either its spectroscopic redshift or its photometric redshift. We neglect the errors on the former and we will discuss the latter further in Sec. III D 2.

The galaxy over-density,  $\delta_g$ , are measured on the redshift slice labeled by  $i$  at the comoving distance  $D_i$  from the observer and is assumed to be a linearly biased tracer of the matter over-density  $\delta_m$ , with bias  $b$ , so that the window function for  $\delta_{i,g}$  is given by

$$W^{i,g}(D_i) = \frac{2}{3} G_{\delta_m}(a_i, k) \frac{dz_i}{dD} n_g(z_i) b(z_i) \frac{(l + 1/2)^2}{\Omega_m H_0^2 D_i^2} \quad (8)$$

where the growth function  $G_{\delta_g}$  is given by  $G_{\delta_g}(a_i, k) = a\Phi(a_i, k)/\Phi(a_0, k)$ .

The deflection angle  $\mathbf{d}$  due to gravitational lensing is defined by the gradient field of the lensing potential,  $\mathbf{d} = \nabla\phi$ , where

$$\phi(z) = -2 \int dD \int_z^\infty dz' n_i(z') \frac{D(z') - D(z)}{D(z)} \phi(a, k). \quad (9)$$

The window function for  $\phi$  is thus

$$W^{i,\phi}(D(z)) = -2G_\Phi(a, k) \int_z^\infty dz' n_i(z') \frac{D(z') - D(z)}{D(z')} \quad (10)$$

where the growth function  $G_\Phi(a, k)$  is given by

$$G_\Phi(a, k) = \Phi(a, k)/\Phi(a_0, k). \quad (11)$$

The angular power spectra of the deflection angle is given by  $C_\ell^{dd} = l(l+1)C_\ell^{i,\phi\phi}$ .

Finally, peculiar velocity in our context will be measured following the method proposed by Song and Percival [46]. On large angular scales, the evolution of LSS measured by peculiar velocity is an independent tracer of the history of LSS. If we consider the energy momentum conservation law written in Eq. 2 to be valid, then the window function for  $\theta_{i,m}$  defined in the  $i^{th}$  shell is given by

$$W^{i,\theta_m}(D_i) = \frac{2}{3} G_{\theta_m}(a_i, k) \frac{dz_i}{dD} n_g(z_i) \frac{(l + 1/2)^2}{\Omega_m H_0^2 D_i^2}, \quad (12)$$

where  $G_{\theta_m} = a\dot{G}_{\delta_m}(a_i, k)$  is the growth factor for  $\theta_m$  and the velocity bias is ignored,  $\theta_{i,g} = \theta_{i,m}$ .

#### B. Redshift distortion and angular power spectra

In this section, we consider a spectroscopic survey whose redshift measurement errors are neglected and discuss the effects of redshift space distortion on the angular power spectra. The galaxy density fluctuations measured

in redshift space are distorted by peculiar velocities on all scales. The observed power spectra can thus be a mixture of density fluctuations and peculiar velocities. To derive the projected galaxy angular power spectra on large scales, i.e. linear, we first write the galaxy density in redshift space as [47]

$$\delta_g(k, \mu, D) = \Phi(k, a_i) W_g(D) (1 + f\mu^2), \quad (13)$$

where curvature perturbations are separated into a scale and a time dependant part,

$$\Phi(k, a) = \Phi_o(k) \frac{\Phi(k, a)}{\Phi(k, a_o)} = \Phi_o(k) a G_{\delta_m}(a), \quad (14)$$

and where  $a_0$  is initial epoch at matter domination and  $G_{\delta_m}$  is growth function of matter fluctuations and the window function  $W_g$  is defined in Eq. 8. The fractional weight function between density fluctuations and peculiar

velocities  $f$  can be written as

$$f = \frac{d \ln G_{\delta_m}(a)}{d \ln a}. \quad (15)$$

The projected 2D galaxy density from redshift space is then written as

$$\begin{aligned} \delta_g(\hat{\mathbf{n}}) &= \int dD W_g(D) (1 + f\mu^2) \delta_{\Phi}(\hat{\mathbf{n}}, D) \\ &= \int dD \int \frac{d^3 \mathbf{k}}{(2\pi)^3} W_g(D) (1 + f\mu^2) \Phi(\mathbf{k}, D) e^{ik\mu D}. \end{aligned} \quad (16)$$

We can then write

$$a_{\ell m}^g = \int d\Omega(\hat{\mathbf{n}}) \delta_g(\hat{\mathbf{n}}) Y_{\ell m}^*(\hat{\mathbf{n}}) \quad (17)$$

hence

$$\begin{aligned} (2\ell + 1) C_{\ell}^{gg} &= \sum_m \langle a_{\ell m}^g a_{\ell m}^{g*} \rangle \\ &= \sum_m \int d\Omega d\Omega' dD dD' \frac{d^3 \mathbf{k}}{(2\pi)^3} \frac{d^3 \mathbf{k}'}{(2\pi)^3} \langle \Phi(\mathbf{k}) \Phi^*(\mathbf{k}') \rangle W_g(1 + f\mu^2) W_g'(1 + f\mu'^2) e^{i(k\mu D - k'\mu' D')} Y_{\ell m}^*(\hat{\mathbf{n}}) Y_{\ell m}(\hat{\mathbf{n}}') \\ &= \sum_m \int \frac{d^3 \mathbf{k}}{(2\pi)^3} P_{\Phi}(k) \left[ \int d\Omega dD W_g(1 + f\mu^2) e^{ik\mu D} Y_{\ell m}^*(\hat{\mathbf{n}}) \right] \left[ \int d\Omega' dD' W_g'(1 + f\mu'^2) e^{ik'\mu' D'} Y_{\ell m}(\hat{\mathbf{n}}') \right]. \end{aligned} \quad (18)$$

We can then calculate the bracket as

$$\begin{aligned} [\dots] &= \int d\Omega dD W_g(1 + f\mu^2) e^{ik\mu D} Y_{\ell m}^*(\hat{\mathbf{n}}) \\ &= \sqrt{\pi(2\ell + 1)} \delta_{m0} \int d\mu dD W_g(1 + f\mu^2) e^{ik\mu D} P_{\ell}(\mu) \\ &= 2\sqrt{\pi(2\ell + 1)} \delta_{m0} \int dD W_g(D) \\ &\times \left[ j_{\ell}(kD) - f \left( j_{\ell-2}(kD) - \frac{\ell}{kD} j_{\ell-1}(kD) \right) \right]. \end{aligned} \quad (20)$$

We thus obtain

$$C_{\ell}^{gg} = 4\pi \int \frac{d^3 \mathbf{k}}{(2\pi)^3} P_{\Phi}(k) [I_{\ell}(k)]^2 \quad (21)$$

where

$$\begin{aligned} I_{\ell}(k) &= \int dD W_g(D) \\ &\times \left[ j_{\ell}(kD) - f \left( j_{\ell-2}(kD) - \frac{\ell}{kD} j_{\ell-1}(kD) \right) \right]. \end{aligned} \quad (22)$$

At high  $\ell$  modes where the Limber approximation is safe, we have  $kD \sim \ell$  which suppresses the contribution from

the  $\Theta\Theta$  modes and we have

$$I_{\ell}(k) \simeq \int dD W_g(D) j_{\ell}(kD), \quad (23)$$

where the redshift distortion effect on the projected power spectra is suppressed.

Those two equations illustrated in Fig. 2 show that projecting the angular power spectrum minimizes the redshift space distortion through cancellation effects. This effect is interesting here since it makes the projected angular density a more direct tracer of the projected matter density. This will not be valid anymore when non-linear effects are non-negligible, that is for scales larger than  $k \sim 0.3 \text{ Mpc}^{-1}$ .

### C. Photometric uncertainties and angular power spectra

We now consider a photometric survey and discuss the effects of redshift errors on the projected galaxy angular power spectrum. We assume for the latter Gaussian error with rms

$$\sigma(z) = \sigma_{\text{phz}}(1 + z). \quad (24)$$

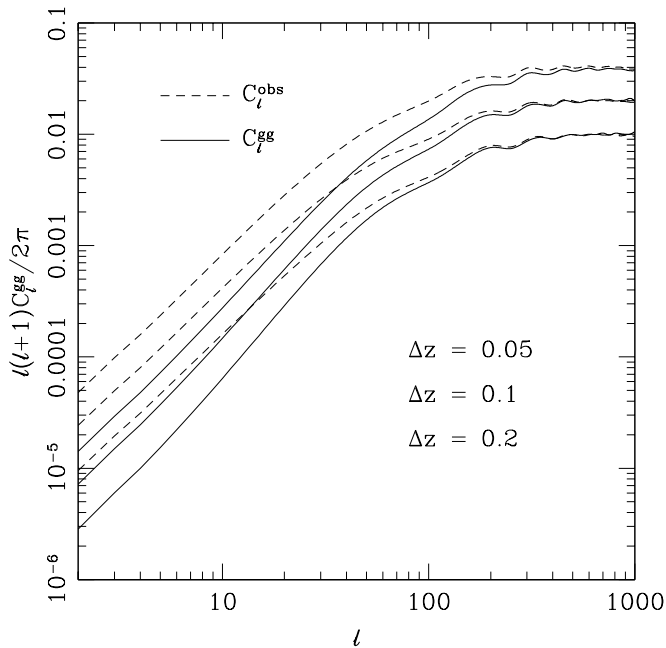


FIG. 2: Projected galaxy over-density angular power spectrum as a function of multipole  $\ell$  as defined in Eq. 21 and Eq. 23 (solid line) and its limber approximation as defined in Eq. 23 (dashed line). The various curves correspond to various bin width. Obviously, the wider the redshift bin the better is the Limber approximation but it is not a very accurate one except at smaller scales.

A subset  $i$  of galaxies whose photometric redshift is such that  $z_{i-1} < z < z_i$ , follows the distribution [48]

$$n_i(z) = \frac{A_i}{2} n_g(z) \left[ \operatorname{erfc} \left( \frac{z_{i-1} - z}{\sqrt{2}\sigma(z)} \right) - \operatorname{erfc} \left( \frac{z_i - z}{\sqrt{2}\sigma(z)} \right) \right],$$

where  $\operatorname{erfc}$  is the complementary error function and  $A_i$  is determined by a normalisation constraint. Throughout this work, we will choose  $A_i$  so that  $\int dz n_i(z) = 1$ . Doing so, we discard the total number of galaxies as an observable.

As an illustration, we consider three different levels of photometric errors, respectively  $\sigma_z = 3 \times 10^{-4}$ ,  $3 \times 10^{-3}$ ,  $3 \times 10^{-2}$ . While the first noise level seems idealistic, the second one seems achievable in a near future (e.g. [49]) and the third one corresponds to what is currently achieved with SDSS [50]. The corresponding window function  $n_g(z)$  defined in Eq. 25 is displayed in the left-top panel of Fig. 3. The left-bottom panel of Fig. 3 shows the simple projected angular power spectra of the galaxy overdensity according to Eq. 6. As we can see, the presence of photometric errors introduces an important error that has to be taken into account.

This error can be simply understood the following way. Looking at the left panel of Fig. 3 one sees that whereas the mean of each distribution and their integral – the total number of galaxies in each bin – are identical, their

variance are widely different. Since the curvature perturbation power spectrum is weighted by the square of  $n_g(z)$  spectrum when Eq. 6 is applied to the galaxy overdensity,  $\delta_g$ , this introduces the substantial bias we see in this plot. If the true underlying distribution was known, i.e. if we could deconvolve the observed distribution with the photometric error distribution, then we could devise easily weights that do not lead to such an error. In practice though, it is unlikely that this deconvolution will be feasible and we thus resort to another way to correct for this effect by introducing another bias factor that we called a photo- $z$  bias,  $b_z$ .

Since  $n_g$  is a smooth function of  $z$  and since the matter power spectrum is mostly featureless, we expect  $b_z$  to be weakly dependent on scales. In the right panel of Fig. 3, we plot the relative difference between the true galaxy angular power spectrum,  $C_\ell^{\text{true}gg}$ , and  $C_\ell^{gg}$  with  $\sigma_z = 0.03$ . In the low redshift bins, there are non-trivial scale dependent in the angular range coming from baryonic features (100Mpc at  $z = 0.3$  corresponds roughly to  $\ell = 60$ ). In the high redshift bins, the scale dependence is ignorable. Fortunately, the contribution from those low redshift bins to the reconstructed lensing power spectra is not significant. It means that we can treat in a first approximation the biasing due to the limited photo- $z$  error as scale independent. Within this hypothesis,  $C_\ell^{gg}$  is a linearly bias tracer of the matter angular power spectrum, with a total bias  $b_T^2 = b_g^2 b_z^2$ , where  $b_g$  denotes the bias due to galaxy and  $b_z$  denote the bias due to photo- $z$  uncertainty. The measure of the 3-D galaxy power spectrum allows us to measure  $b_g$  separately but we can also measure directly the total bias in a redshift bin,  $i$ , as will be detailed in Sec. III D 2.

#### D. Galaxy bias and associated uncertainties

We now present two alternative ways to measure the linear galaxy bias, assuming either a precise spectroscopic survey or a weak-lensing based photometric survey.

##### 1. Using a spectroscopic survey

Using precise spectroscopic redshift measurements, we are able to separate the peculiar velocity power spectra from the redshift-space power spectrum  $P_g^{\text{obs}}(\mathbf{k})$  of a galaxy redshift survey [46]. The latter is commonly modeled as

$$P_g^{\text{obs}}(\mathbf{k}) = \left[ P_{gg}(\mathbf{k}) + 2\mu^2 P_{g\Theta_g}(\mathbf{k}) + \mu^4 P_{\Theta_g\Theta_g}(\mathbf{k}) \right] \times F(k^2 \sigma_v^2(z) \mu^2). \quad (25)$$

The separation of  $P_{gg}(\mathbf{k})$  and  $P_{\Theta\Theta}(\mathbf{k})$  made possible using the angular dependence of  $P_g^{\text{obs}}(\mathbf{k})$  and where  $\Theta = \theta/aH$  [51].

We quantify how well this separation can be performed using a Fisher matrix formalism. The Fisher matrix anal-

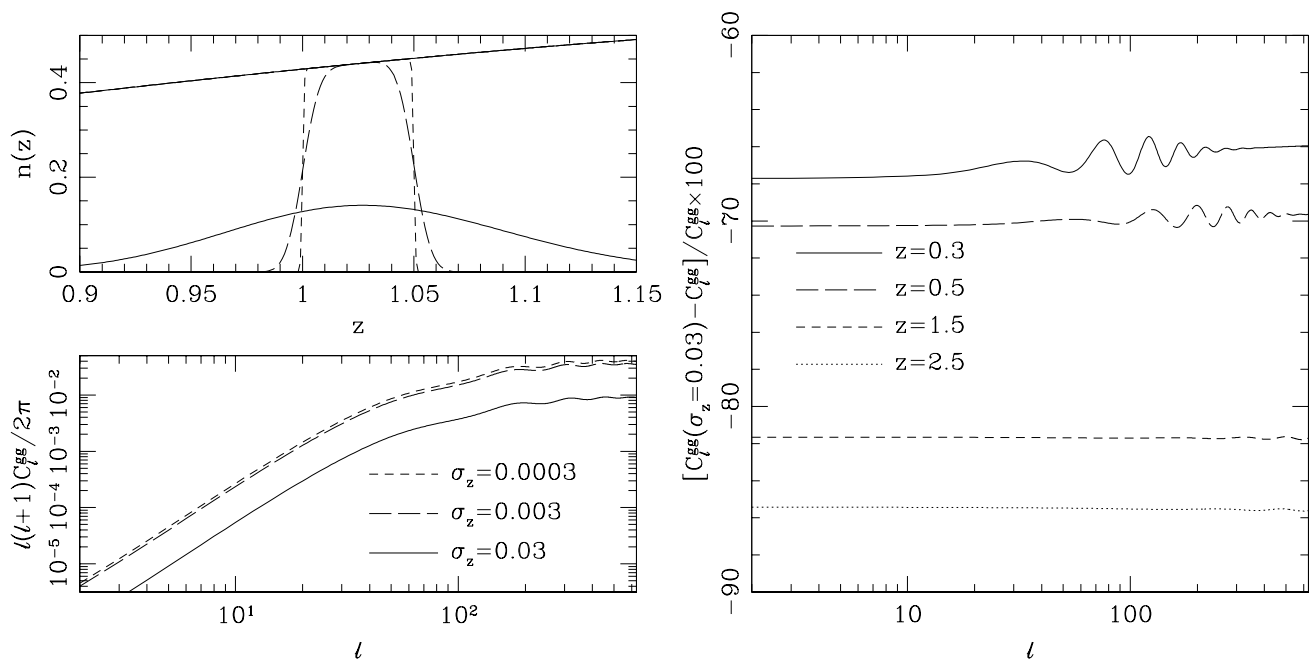


FIG. 3: *Left panel, top*:  $n_g$  distribution plotted for three various  $\sigma_z$ , i.e.  $3 \times 10^{-4}$ ,  $3 \times 10^{-3}$ ,  $3 \times 10^{-2}$  and the underlying galaxy distribution. *Bottom*: Corresponding galaxy overdensity angular power spectrum,  $C_l^{gg}$ . Photometric redshift error entails an important bias. *Right panel*: Relative difference between  $C_l^{gg}$  power spectra with or without photo- $z$  errors considering  $\sigma_z = 0.03$ . Solid, long dash, short dash and dotted curves correspond respectively to  $C_l^{gg}$  at  $z=0.3, 0.5, 1.5$  and  $2.5$ .

ysis relevant to this separation for a given  $k$  and  $z$  bin is given by [51]

$$F_{\alpha\beta}(k_i, z_j) = \int_{k_i^{\min}}^{k_i^{\max}} \frac{k^2 dk}{2(2\pi)^2} \int_{-1}^1 d\mu V_{\text{eff}}(k, \mu, z_j) \times \frac{\partial \ln P_g^{\text{obs}}(k, \mu, z_j)}{\partial p_\alpha} \frac{\partial \ln P_g^{\text{obs}}(k, \mu, z_j)}{\partial p_\beta} w_{F_{oG}}(k, \mu) \quad (26)$$

where  $\alpha$  and  $\beta$  run from 1 to 2 and denote respectively  $P_{gg}$  and  $P_{\Theta\Theta}$  and  $w_{F_{oG}}$  is a down-weight function filtering out the modes contaminated by non-linear redshift space distortions. Note that  $P_{g\Theta_g}$  is considered to be 1 in this separation which is valid on the linear scales of interest to us. The effective volume  $V_{\text{eff}}^j$  in each redshift bin  $j$  is

$$V_{\text{eff}}(k_i, \mu, z_j) = \left[ \frac{n^j P_g^{\text{obs}}(k_i, \mu, z_j)}{n^j P_g^{\text{obs}}(k_i, \mu, z_j) + 1} \right]^2 V_{\text{survey}}(z_j) \quad (27)$$

where  $n^j$  is the shot noise term coming from the finite galaxy density supposed constant here, and  $V_{\text{survey}}(z_j)$  is the survey volume in a given redshift bin. For the large scales of interest to us, the cosmic variance term dominates over the shot noise and  $V_{\text{eff}}(k_i, \mu, z_j)$  is nearly identical to  $V_{\text{survey}}(z_j)$ . For our estimation, we will consider a full sky survey with a constant galaxy density of  $\bar{n} = 5 \times 10^{-3} h^3 \text{Mpc}^{-3}$  and a constant bias equals to

1. As illustrated in left panels of Fig. 4, we are able to separate properly  $P_{gg}$  and  $P_{\Theta\Theta}$  for wide  $k$  and  $z$  bins.

Following this measurement of  $P_{gg}$  and  $P_{\Theta\Theta}$ , we can constrain simultaneously the cosmological parameters and the galaxy biases. If the galaxy bias is scale-independent and depends only on redshift, then the real space galaxy power spectrum  $P_{gg}$  can also be written in terms of the fundamental cosmological parameters plus a vector of bias parameters. If we consider for example a survey up to  $z = 3.2$  with 8 redshift bins of width  $\Delta z = 0.4$ , the standard DE cosmological parameter set – as the one used in the Dark Energy Task Force report [52] – is extended to 16 elements,  $q = (w, w_a, w_m, w_b, A_S, n_S, z_{\text{reion}}, \theta_S, b_{j=1-8})$ . For this extended cosmological space, the Fisher matrix simply writes

$$F_{mn} = \sum_{ij} \sum_{\alpha\beta} \frac{\partial p_\alpha}{\partial q_m} F_{\alpha\beta}(k_i, z_j) \frac{\partial p_\beta}{\partial q_n}. \quad (28)$$

Since  $P_{\Theta\Theta}$  is independent of bias, the degeneracy between cosmological parameters and the bias is broken [53], and we can simultaneously measure in each redshift bin the bias and e.g. the dark energy parameters. The resulting bias uncertainties are given for each redshift bin in Table IIID 1 and are typically at the percent level. Note that the galaxy bias measurement is not detrimental to the dark energy parameters as illustrated in the right panels of Fig. 4.

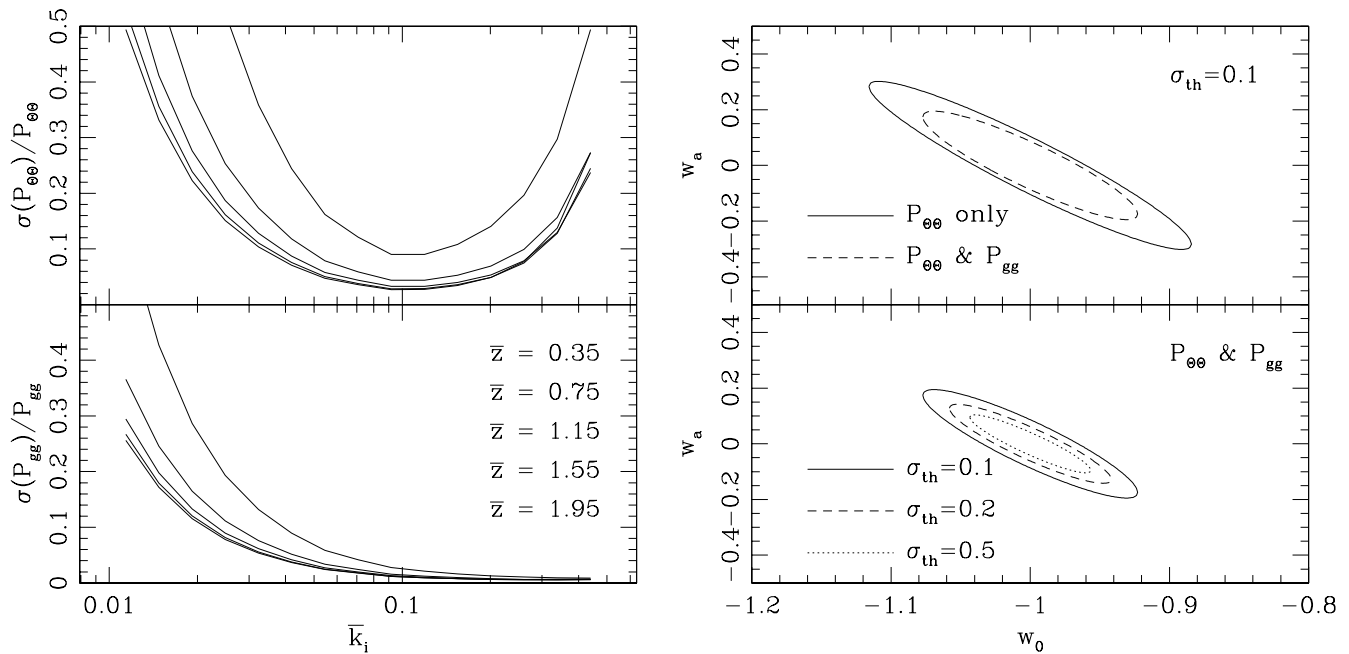


FIG. 4: *Left panels:* The top panel show the fractional errors for the reconstructed  $P_{\Theta_g\Theta_g}$  using the Fisher matrix formalism written in Eq. 26. The bottom plot shows the corresponding fractional errors for  $P_{gg}$ . *Right panels:* 68% CL contour plots in the  $w - w_a$  plane. The top panel shows the constraints obtained using  $P_{\Theta_g\Theta_g}$  (no bias marginalization) only and  $P_{\Theta_g\Theta_g} + P_{gg}$  (with bias marginalization). The bottom panel shows the constraints using  $P_{\Theta_g\Theta_g} + P_{gg}$  and various value of the parameters  $\sigma_{th}$  that quantifies the accuracy of the modeling of the Finger of God effect (see Eq. 15 of White et al. [51] for details).

TABLE I: The fractional error of bias in some selected redshift bins using Eq.28.

$z_j$	0.05	0.55	1.05	1.55	2.05	2.55	3.05
$\frac{\Delta b_j}{b_j} (\%)$	0.75	0.37	0.33	0.38	0.45	0.53	0.57

## 2. Using a photometric survey

As introduced earlier, redshift uncertainties as big as the ones resulting from photometric redshift measurements introduce an extra, almost linear bias,  $b_z$ . Since this bias does not affect the cross-correlation between galaxy and peculiar velocity, we can only determine the “total bias” by cross-correlating the weak gravitational lensing signal and the projected galaxy density. The signal-to-noise ratio for this correlation is simply given by [54]

$$\left(\frac{S}{N}\right)_j^2 = \sum_{s=1}^8 \sum_{l=l_{\min}}^{l_{\max}} \frac{f_{\text{sky}}(2l+1)(C_\ell^{\delta_g^j d_s})^2}{(C_\ell^{\delta_g^j \delta_g^j} + N_\ell^{\delta_g^j \delta_g^j})(C_\ell^{d_s d_s} + N_\ell^{d_s d_s})}, \quad (29)$$

and the fractional error on the galaxy bias is

$$\frac{\Delta b_t}{b_t} = \frac{1}{S/N}. \quad (30)$$

Some promising SNR numbers are given in Tab. II where we used all the  $\ell$  up to  $\ell = 500$ , assumed  $\sigma_z = 0.03$  and considered a redshift binning for the WL signal from  $z=0$  to 3.2 with  $\Delta z = 0.4$ . Note that for this evaluation, unlike in the previous section we did not vary the other cosmological parameters but here again, we expect the DE parameters to be non-degenerate with the bias when we include the the projected galaxy and weak gravitational lensing cross-correlation.

TABLE II: Signal to noise ratio estimate for the total bias as defined in Eq. 29 in selected bins.

$z_j$	0.05	0.55	1.05	1.55	2.05	2.55	3.05
$(S/N)_j$	160	430	300	170	88	35	6.6
$\Delta b_j/b_j (\%)$	0.63	0.23	0.33	0.58	1.1	2.8	15

## IV. CONSISTENCY TESTS

Now that we have presented how to obtain accurate estimates of the projected matter angular power spectrum using galaxy surveys, we proceed to the core of our study, that is the details of our cosmological consistency tests. We will propose two tests. Either we predict the lensing convergence power spectra using a galaxy survey

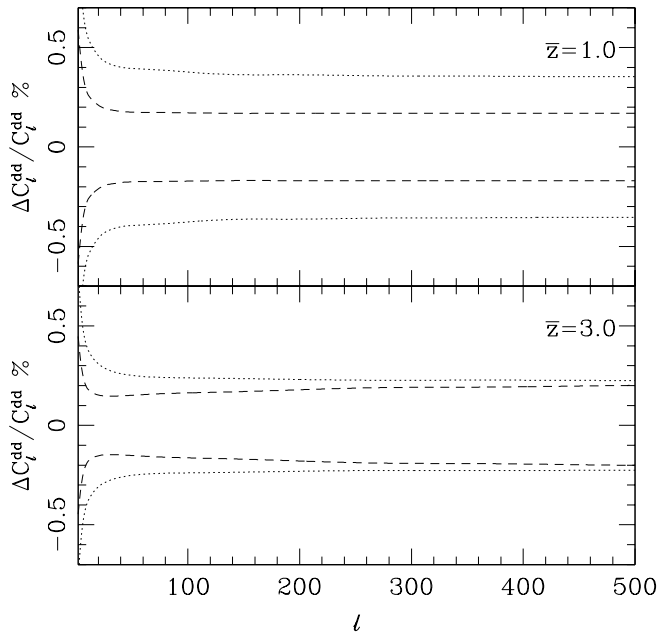


FIG. 5: Relative uncertainties for the reconstructed  $C_l^{dd}$ . The dash line corresponds to the statistical uncertainties when measuring the bias using a large spectroscopic survey (as in Sec. III D 1) and the dotted line corresponds to the statistical uncertainties when using a photometric survey (as in Sec. III D 2). Other systematic bias are illustrated in Fig. 6.

and compare it to the measured lensing power spectra, or we predict the cross-correlation between matter and galaxy. While the first constitutes an observational implementation of both the *metric test* written in Eq. 3 and the *non-dynamical constrain test*, the second one is a direct implementation of the *non-dynamical constrain test* written in Eq. 5.

### A. Predicting the lensing power spectra

The density perturbations are measured on the redshift shell labeled by  $i$  at the comoving distance  $D_i$  from the observer. In the approximation of a quasi-static evolution of perturbations, i.e. considering the perturbations constant within a redshift shell, the projected angular power spectrum can be written as

$$C_l^{i\,gg} = \frac{2\pi^3}{(l+1/2)^3} \Delta D_i D_i W^g(D_i) W^g(D_i) \Delta_{\Phi\Phi}(a_i, k). \quad (31)$$

Similarly, the weak lensing power spectra can be discretized as

$$C_l^{s\,dd} = \frac{2\pi^2}{l+1/2} \sum_{i=1}^n \Delta D_i D_i \frac{4(D_s - D_i)^2}{D_s^2 D_i^2} \Delta_{\Phi\Phi}(a_i, k) \quad (32)$$

If we first assume that there is no dark energy perturbations, then  $\Delta_{\Phi\Phi}(a_i, k)$  can be written in terms of the

angular power spectrum of galaxies within this shell as

$$\Delta_{\Phi\Phi}^i = \frac{9}{8\pi^2(l+1/2)} \frac{D_i^3}{\Delta D_i} \left( \frac{dz}{dD} n_i b_i \right)^{-2} \frac{\Omega_m^2 H_0^4}{a_i^2} C_l^{i\,gg}. \quad (33)$$

Substituting this into Eq. (32), we are lead to define the reconstructed lensing power spectra

$$\tilde{C}_l^{s\,dd} = \sum_{i=1}^n \frac{1}{b_i^2} F_l^i \quad (34)$$

$$F_l^i = \frac{9}{(l+1/2)^2} \frac{D_i^2 (D_s - D_i)^2}{D_s^2} \left( \frac{dz}{dD} n_i \right)^{-2} \frac{\Omega_m^2 H_0^4}{a_i^2} C_l^{i\,gg}.$$

Note that this estimator is the simplest we can devise and that we considered the noise to be negligible. We also ignore correlations within redshift bins, which is true if they are wide enough. If these hypothesis are not fulfilled, it is straightforward to generalize our estimator to handle those effects in an optimal manner. In Fig. 5 we show the statistical errors for the reconstructed power spectra using our nominal survey. Obviously, the reconstruction performs very well. In the right panel of Fig. 6, we plotted several reconstructed power spectra, before and after photo-z bias reconstruction for  $\Delta z = 0.4$  bins and photo-z errors defined by  $\sigma_z = 0.03$ . Obviously, the reconstructed estimator agrees well with the input ones once corrected from the photo-z bias. As expected following the results of Fig. 3 though, this bias is harder to correct at low  $z$ .

Once this estimator is defined, we can calculate the variance of  $\Delta \tilde{C}_l^{s\,dd}$  as

$$\Delta \tilde{C}_l^{s\,dd} = \left\{ \sum_{i=1}^n \left[ \frac{1}{b_i^2} F_l^i \left( 2 \frac{\Delta b_i}{b_i} \right) \right]^2 \right\}^{1/2} \quad (35)$$

which gives a fractional error

$$\frac{\Delta \tilde{C}_l^{s\,dd}}{\tilde{C}_l^{s\,dd}} = \frac{\left\{ \sum_{i=1}^n \left[ \frac{1}{b_i^2} F_l^i \left( 2 \frac{\Delta b_i}{b_i} \right) \right]^2 \right\}^{1/2}}{\sum_{i=1}^n \frac{1}{b_i^2} F_l^i}. \quad (36)$$

We show the predicted lensing signal accuracy in Fig. 6 using the same survey parameters as for Fig. 4. The resulting statistical uncertainties in the predicted angular power spectrum (right panel) are much smaller than the potential reconstruction biases from non-linear effect, limited photometry measurement accuracy and discreteness effects. Percent accuracy is still possible with coming surveys and we will discuss further in Sec. V the subsequent cosmological interpretation.

The number of galaxy redshift bins used to approximate the continuous kernel of lensing potential along the line of sight in Eq. 34 is limited. The choice of the optimal bin width is motivated by several issues. We chose the thickness of the bins to be larger than any correlation length between two subsequent bins. Besides, since



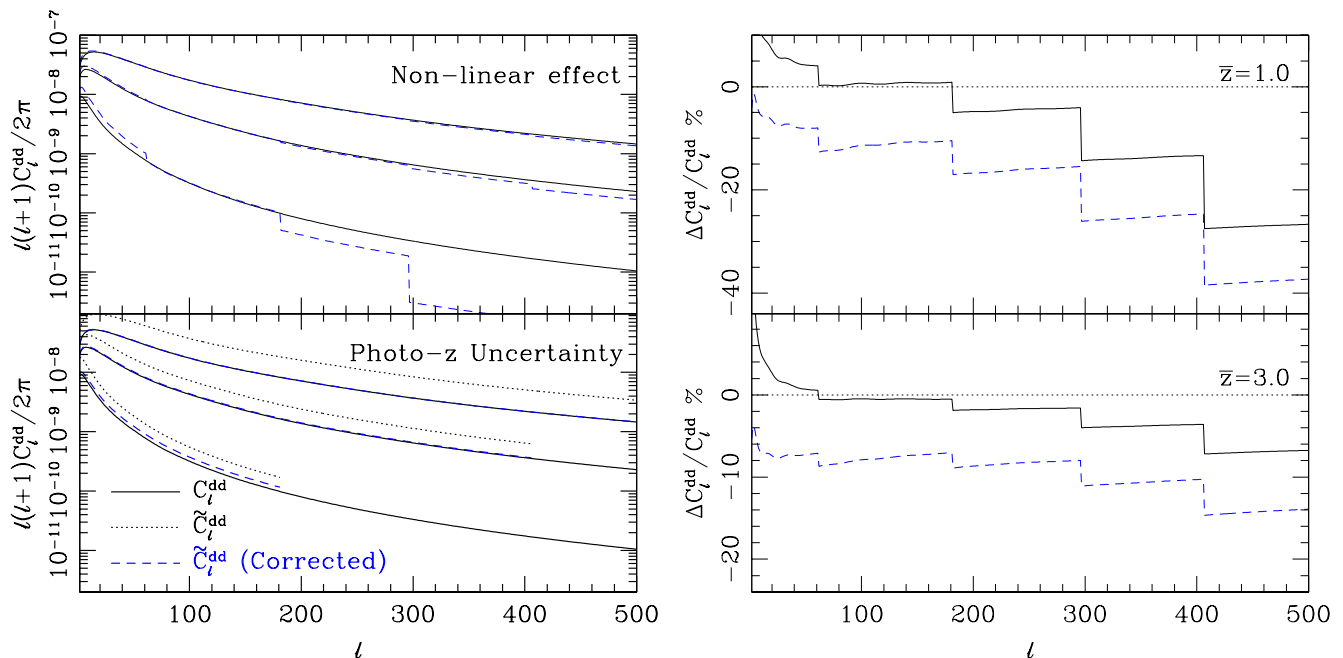


FIG. 6: *Left panel:*  $C_l^{dd}$  for a source distribution at  $\bar{z}=0.2, 1.0$  and  $3.0$  (from bottom to top) with a redshift width  $\Delta z = 0.4$ . (*top panel*) The solid curves represent the original WL power spectra, and the dash curves represent the reconstructed one when the projected galaxy angular power spectra have been cut below some non-linear threshold chosen here to be  $k \sim 0.3 Mpc^{-1}$ . (*bottom panel*) The solid curves represent the original WL power spectra, the dotted curves represent the reconstructed ones with photo- $z$  error of  $\sigma_z = 0.03$  and the dash curves represent the predicted ones corrected for the photo- $z$  bias. The agreement is obviously good except at low  $z$  where the photo- $z$  bias is harder to correct for. *Right panel:* Expected relative uncertainties in the lensing predicted angular power spectra for the source distribution at two various redshifts ( $1.0$  and  $3.0$  respectively from top to bottom panels and again  $\Delta z = 0.4$ ). The thin curves represent the reconstructed lensing signal using all the information available from the projected galaxy density. The visible noise at low  $\ell$  originates in the finite number of galaxy redshift bins available. The thick curves is obtained when removing all the galaxy information above  $k \sim 0.3 Mpc^{-1}$  to stay in the linear regime. The black curves correspond to the reconstruction for a  $\Lambda$ CDM model. The blue curves to the reconstruction for  $f(R)$  gravity with  $B_0 = 1$  (see Sec. V for more details). Whereas the reconstruction performs really well in the

the projected galaxy angular power spectra are defined in redshift space, a larger width smooth the redshift distortion effect as shown in Fig. 2. We find a width of roughly  $\Delta z = 0.1$  to be satisfying. The thin curves in the right panel of Fig. 6 shows that whereas the accuracy of  $\bar{C}_l^{dd}$  at  $\bar{z} = 0.2$  is limited by discreteness effect (we can use only 4  $z$  bins), it is nearly ignorable at high redshift lensing bins.

Another important bias factor involves non-linear effects. Whereas the Poisson equation we used to predict the lensing signal is valid on all scales, to reconstruct a reliable projected density template from the galaxies measured in redshift space might be challenging in the non-linear regime. To illustrate how important this effect is, we filter out the galaxy template for  $k < 0.3 h/Mpc$  and then project the galaxy density field. In the right panel of Fig. 6, the stepwise curves represent the resulting predicted lensing signal. Because non-linearities are stronger at low redshift, this bias is more important when predicting the lensing signal at lower redshift.

The uncertainty due to photometry measurement can be another significant bias as shown in the left-bottom panel of Fig. 6. However, we presented in Sec. III D 2 how

to deal with such an effect using spectroscopic surveys or photometric surveys. This bias should thus not be a practical application of our test.

## B. Adding cross-correlation with velocity

In addition to the comparison between the predicted and the measured lensing power spectra at various redshifts, we can devise another consistency test using cross-correlations between galaxy and weak lensing. This test will highlight in particular any deviation from the Poisson equation that we parametrize with the  $\alpha$  parameter defined by

$$k^2 \Phi = 4\pi G_N \alpha a^2 \rho_m \delta_m . \quad (37)$$

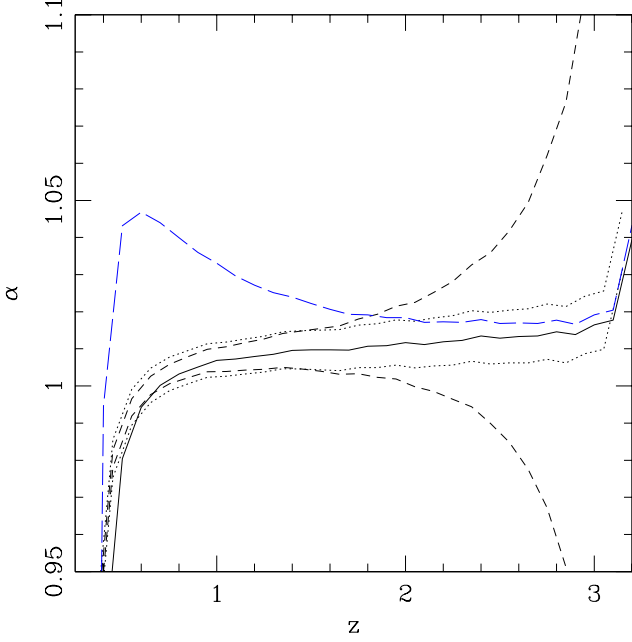


FIG. 7: Black solid curve represent  $\alpha_i$  for  $\Lambda$ CDM and blue solid curve represent  $\alpha_i$  for f(R) theories with  $B_0 = 1$ . Dash curves are errors estimated when using WL-galaxy correlations (as in Sec. III D 2) and dotted curves are error estimated using the galaxy-peculiar velocity correlations (as in Sec. III D 1).

$\alpha = 1$  corresponds to GR. An estimator for  $\alpha$  can be simply derived using  $C_\ell^{d\delta_g}$  and  $C_\ell^{\delta_g\delta_g}$ , that we rewrite as

$$C_\ell^{d\delta_g} = \frac{2\pi^3}{l^2} \Delta D_i D_i \left( -2G_\Phi \frac{D_s - D_i}{D_s D_i} \right) \times \frac{2}{3} G_\Phi \frac{dz}{dD} n_i b_i \frac{al^2}{\alpha \Omega_m H_0^2 D_i^2} \frac{9}{25} \Delta \zeta \zeta \quad (38)$$

$$C_\ell^{\delta_g\delta_g} = \frac{2\pi^3}{l^3} \Delta D_i D_i \left( \frac{2}{3} G_\Phi \frac{dz}{dD} n_i b_i \frac{al^2}{\alpha \Omega_m H_0^2 D_i^2} \right)^2 \frac{9}{25} \Delta \zeta \zeta \quad (39)$$

The estimator  $\alpha_i$  is given by,

$$\alpha_i = - \frac{dz}{dD} n_i b_i \frac{l^2}{3\Omega_m H_0^2 D_i} \frac{D_s}{D_s - D_i} \frac{C_\ell^{d\delta_g}}{C_\ell^{\delta_g\delta_g}}.$$

As such, the fractional error for  $\alpha_i$  is equivalent to the fractional error for  $b_i$  given in Tab. III D 1,

$$\frac{\Delta \alpha}{\alpha} = \frac{\Delta b_i}{b_i} \quad (40)$$

and also we can also relate it directly to the compare it with the fractional error of  $\tilde{C}_l^{sdd}$  using Eq.36.

In Fig. 7, the estimated  $\alpha$  from galaxy maps and cross correlation with lensing potential is presented. Solid curve is the estimated  $\alpha$  which departs from unity around edges of lensing kernel sourced by galaxies at  $\bar{z} = 3.0$ .

But the estimation of  $\alpha$  is very close to what is expected from GR model, unity. Due to diverse bias effect, it is not identical to unity, but it is just off by a percentage level. Still the difference due to systematic effect is much smaller than the theoretical deviation due to violated GR assumptions, e.g  $f(R)$  (R:Ricci scalar) gravity model with  $B_0 = 1$  (long dash curve in Fig. 7), where  $B_0$  is defined as,

$$B_0 = \frac{d^2 f/dR^2}{1 + df/dR} \frac{dR}{d \ln a} \left( \frac{d \ln H}{d \ln a} \right)^{-1}. \quad (41)$$

Dash and dotted curves are statistical errors from different galaxy bias estimation from redshift survey alone and cross-correlations. The advantage of this test over reconstructed  $\tilde{C}_l^{dd}$  is that we are able to see tomographic view of consistency relation.

## V. DISCUSSION

In this paper, we advocate the use of consistency relations to test gravity on cosmological scales. We did so by using a combination of observables. This approach remains model independent and does not rely on any specific parametrization. We focused in particular on the joint use of galaxy surveys and weak-lensing observables. We showed how using the former to predict the latter, we can build a strong self-consistency test for GR. We also showed how large-scale redshift surveys can be extremely valuable in such an endeavor. The test we proposed seems particularly appealing since any weak-lensing survey is also by nature a galaxy clustering survey and we illustrated how even a photo-z survey can be used to build a strong self-consistency test. We thus expect this test to be applied in the near future to the CFHTLS survey [63] and others like DES [64], the proposed JDEM [65] and Euclid [66] space missions.

We address in this work the key observational and astrophysical systematics like the galaxy bias and redshift uncertainties but many more survey specific ones would have to be carefully studied before any conclusion can be drawn from any particular data-sets, e.g.  $n(z)$  errors, PSF correction and variation over large scales. It is quite likely that this kind of test will be ultimately limited by the level of control of systematics. In particular, we purposefully worked on linear scales. Non-linear effects in real and redshift space will limit the useful scales for such a program. If we assume that we can handle non-linear effects up to  $k=0.3 h/\text{Mpc}$ , we can see in the left panel of Fig. 4 that our program is still tractable. Besides, weak-gravitational lensing has now been measured in the linear regime where this test could be applied [55]. Another unexplored sides of our work lie in the possible degeneracies with underlying cosmological model parameters but we leave this study for future work.

More positively, although, our survey parametrization is quite generic, these surveys could certainly be customized to enhance the discriminatory power of this test

and others. We encourage future missions to include the feasibility of such tests as an extra criteria in the optimization of their design.

Assuming that all systematics are well under control, we can wonder what new physics can be probed with this test. As an illustration, we plotted in Fig. 6 the predictions for a  $f(R)$  theory where a non-linear function  $f$  of the Ricci scalar  $R$  is added to the Einstein-Hilbert action [56]. We considered typical value of the dimensionless Compton wavelength parameter  $B_0 = 1$  (see Eq. 17 in [56]). In  $f(R)$  gravity models, the Poisson equation is modified so that  $G_N \rightarrow G_N/(1 + df/dR)$  and a non-zero anisotropy stress is introduced to break the simplest GR model anisotropy condition  $\Phi = -\Psi$ . As visible in Fig. 6, the predicted  $\bar{C}_l^{dd}$  for a  $f(R)$  gravity model using GR assumptions would differ from the observed one at a level well exceeding the various potential biases. This discrepancy originates from the GR assumption in Eq. 34 since any non-zero anisotropic stress invalidates the relation  $2\Phi = \Phi - \Psi$ . However, the reduced mass scale affecting  $f(R)$  theories modify the Poisson equation. It can thus be probed directly using the cross-correlation technique detailed in Sec. IV B. Note that since the difference between this  $f(R)$  model and GR increases when the redshift decreases, so does the discrepancy between the observed and predicted  $C_l^{dd}$  for a  $f(R)$  theory. From the Fig. 7 it can be seen that constraints on  $B_0$  of order 1 or less are in principle feasible with such a test. Other aspects of  $f(R)$  theories are discussed in [57, 58, 59].

More generally, it can be argued that any theory with non-minimal interaction in the dark sector or dark energy clumping would fail this test since it either modifies the Poisson equation or introduce an anisotropic stress [32, 60]. Conversely, it is important to note that some types of modified gravity models would pass the test we detailed here. For example, the potentials following from a DGP model [61] are modified in such a way that the light path tracing potential differences is similar to the standard  $\Lambda$ CDM predictions. To detect such models, we need to implement the program proposed in [42].

The tests presented above are only two of examples of the possible one highlighted in Sec. II and we plan to extend our studies to include other consistency relations as well as other observables like the integrated Sachs-Wolfe effect [62] and the lensing of the cosmic microwave background. We believe however that the observational program sketched in this paper already offers a stringent observational test of GR and we thus plan to put it into action using current data.

### Acknowledgments

We thank Pat McDonald for useful discussions and Jean-Philippe Uzan for a careful reading of a draft version of this paper. YSS is supported by STFC.

- 
- [1] A. G. Riess et al. (Supernova Search Team), *Astrophys. J.* **607**, 665 (2004), astro-ph/0402512.
  - [2] P. Astier et al. (The SNLS), *Astron. Astrophys.* **447**, 31 (2006), astro-ph/0510447.
  - [3] D. J. Eisenstein et al. (SDSS), *Astrophys. J.* **633**, 560 (2005), astro-ph/0501171.
  - [4] S. Cole et al. (The 2dFGRS), *Mon. Not. Roy. Astron. Soc.* **362**, 505 (2005), astro-ph/0501174.
  - [5] M. Tegmark et al., *Phys. Rev.* **D74**, 123507 (2006), astro-ph/0608632.
  - [6] E. Komatsu et al. (WMAP) (2008), 0803.0547.
  - [7] M. Kilbinger et al. (2008), 0810.5129.
  - [8] P. J. E. Peebles and B. Ratra, *Rev. Mod. Phys.* **75**, 559 (2003), astro-ph/0207347.
  - [9] R. Durrer and R. Maartens (2008), 0811.4132.
  - [10] E. G. Adelberger, B. R. Heckel, and A. E. Nelson, *Annual Review of Nuclear and Particle Science* **53**, 77 (2003), hep-ph/0307284.
  - [11] C. Quercellini, M. Quartin, and L. Amendola (2008), 0809.3675.
  - [12] J. Goodman, *Phys. Rev.* **D52**, 1821 (1995), astro-ph/9506068.
  - [13] R. R. Caldwell and A. Stebbins, *Phys. Rev. Lett.* **100**, 191302 (2008), 0711.3459.
  - [14] J.-P. Uzan, C. Clarkson, and G. F. R. Ellis, *Phys. Rev. Lett.* **100**, 191303 (2008), 0801.0068.
  - [15] M. Ishak, A. Upadhye, and D. N. Spergel, *Phys. Rev.* **D74**, 043513 (2006), astro-ph/0507184.
  - [16] Y.-S. Song, *Phys. Rev.* **D71**, 024026 (2005), astro-ph/0407489.
  - [17] S. Wang, L. Hui, M. May, and Z. Haiman, *Phys. Rev.* **D76**, 063503 (2007), 0705.0165.
  - [18] L. Knox, Y.-S. Song, and J. A. Tyson, *Phys. Rev.* **D74**, 023512 (2006).
  - [19] M. J. Mortonson, W. Hu, and D. Huterer (2008), 0810.1744.
  - [20] O. Doré and Y.-S. Song, in preparation (2008).
  - [21] E. V. Linder, *Phys. Rev.* **D72**, 043529 (2005), astro-ph/0507263.
  - [22] E. V. Linder and R. N. Cahn, *Astropart. Phys.* **28**, 481 (2007), astro-ph/0701317.
  - [23] D. Huterer and E. V. Linder, *Phys. Rev.* **D75**, 023519 (2007), astro-ph/0608681.
  - [24] D. Polarski and R. Gannouji, *Phys. Lett.* **B660**, 439 (2008), 0710.1510.
  - [25] C. Di Porto and L. Amendola, *Phys. Rev.* **D77**, 083508 (2008), 0707.2686.
  - [26] S. A. Thomas, F. B. Abdalla, and J. Weller (2008), 0810.4863.
  - [27] J. B. Dent and S. Dutta (2008), 0808.2689.
  - [28] J.-P. Uzan and F. Bernardeau, *Phys. Rev. D* **64**, 083004 (2001), hep-ph/0012011.
  - [29] Y.-S. Song (2006), astro-ph/0602598.
  - [30] E. Bertschinger, *Astrophys. J.* **648**, 797 (2006), astro-ph/0604485.
  - [31] T. Koivisto and D. F. Mota, *Phys. Rev.* **D73**, 083502

- (2006), astro-ph/0512135.
- [32] L. Amendola, M. Kunz, and D. Sapone, *JCAP* **0804**, 013 (2008), 0704.2421.
- [33] J.-P. Uzan, *Gen. Rel. Grav.* **39**, 307 (2007), astro-ph/0605313.
- [34] W. Hu and I. Sawicki, *Phys. Rev.* **D76**, 104043 (2007), 0708.1190.
- [35] W. Hu, *Phys. Rev.* **D77**, 103524 (2008), 0801.2433.
- [36] G.-B. Zhao, L. Pogosian, A. Silvestri, and J. Zylberberg (2008), 0809.3791.
- [37] E. Bertschinger and P. Zukin, *Phys. Rev.* **D78**, 024015 (2008), 0801.2431.
- [38] S. F. Daniel, R. R. Caldwell, A. Cooray, and A. Melchiorri, *Phys. Rev.* **D77**, 103513 (2008), 0802.1068.
- [39] R. Caldwell, A. Cooray, and A. Melchiorri, *Phys. Rev.* **D76**, 023507 (2007), astro-ph/0703375.
- [40] O. Dore et al. (2007), 0712.1599.
- [41] B. Jain and P. Zhang (2007), arXiv:0709.2375 [astro-ph].
- [42] Y.-S. Song and K. Koyama (2008), 0802.3897.
- [43] P. Zhang, M. Liguori, R. Bean, and S. Dodelson, *Phys. Rev. Lett.* **99**, 141302 (2007), 0704.1932.
- [44] P. Zhang, R. Bean, M. Liguori, and S. Dodelson (2008), 0809.2836.
- [45] G. M. Bernstein and B. Jain, *Astrophys. J.* **600**, 17 (2004), astro-ph/0309332.
- [46] Y.-S. Song and W. J. Percival (2008), 0807.0810.
- [47] N. Kaiser, *Mon. Not. Roy. Astron. Soc.* **227**, 1 (1987).
- [48] Z.-M. Ma, W. Hu, and D. Huterer, *Astrophys. J.* **636**, 21 (2005), astro-ph/0506614.
- [49] N. Benitez et al. (2008), 0807.0535.
- [50] N. Padmanabhan et al. (SDSS), *Mon. Not. Roy. Astron. Soc.* **359**, 237 (2005), astro-ph/0407594.
- [51] M. White, Y.-S. Song, and W. J. Percival (2008), 0810.1518.
- [52] A. Albrecht et al. (2006), astro-ph/0609591.
- [53] Y.-S. Song, W. J. Percival, and M. White, in preparation (2008).
- [54] V. Acquaviva, A. Hajian, D. N. Spergel, and S. Das, *Phys. Rev.* **D78**, 043514 (2008), 0803.2236.
- [55] L. Fu et al. (2007), 0712.0884.
- [56] Y.-S. Song, W. Hu, and I. Sawicki, *Phys. Rev.* **D75**, 044004 (2007), astro-ph/0610532.
- [57] A. Cooney, S. DeDeo, and D. Psaltis (2008), 0811.3635.
- [58] R. Gannouji, B. Moraes, and D. Polarski (2008), 0809.3374.
- [59] S. Nojiri and S. D. Odintsov (2008), 0807.0685.
- [60] M. Kunz and D. Sapone, *Phys. Rev. Lett.* **98**, 121301 (2007), astro-ph/0612452.
- [61] G. Dvali, G. Gabadadze, and M. Porrati, *Physics Letters B* **485**, 208 (2000), hep-ph/0005016.
- [62] R. K. Sachs and A. M. Wolfe, *Astrophys. J.* **147**, 73 (1967).
- [63] <http://www.cfht.hawaii.edu/Science/CFHLS/>
- [64] <https://www.darkenergysurvey.org/>
- [65] <http://jdem.gsfc.nasa.gov/>
- [66] <http://sci.esa.int/science-e/www/object/index.cfm?fobjectid=42266>